

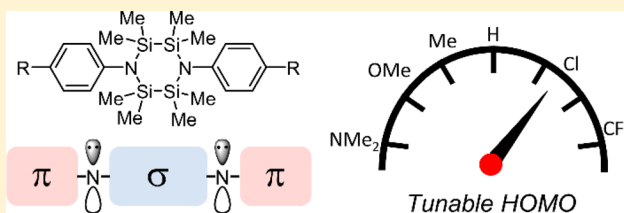
Tunable SiN Hybrid Conjugated Materials

Carlton P. Folster, Phi N. Nguyen, Maxime A. Siegler,^{1b} and Rebekka S. Klausen^{*1b}

Department of Chemistry, Johns Hopkins University, 3400 North Charles Street, Baltimore, Maryland 21218, United States

Supporting Information

ABSTRACT: We report the synthesis of a family of N-aryl cyclosilazanes. The reaction of 1,2-bis(trifluoromethanesulfonate)tetramethyldisilane with *para*-substituted anilines gives six-membered rings with no observed condensation polymerization. X-ray crystallography reveals the cyclosilazane adopts a twist boat conformation with both nitrogens in a trigonal planar geometry. Solution phase UV–vis spectroscopic studies coupled with density functional theory calculations interrogate the ability of the nitrogen atom to bridge the σ - and π -conjugated moieties. Depending on the aromatic substituent, the cyclosilazane rings may be either more or less electron rich than an all silicon ring.



INTRODUCTION

Heteroatom incorporation tunes the properties and function of a conjugated material.¹ A fundamental understanding of the effect of heteroatom incorporation is essential for rational design.^{2–4} Group 15 elements (e.g., nitrogen, phosphorus) combined with π -conjugated systems can act either in an electron-withdrawing or in an electron-donating sense depending on the competing influence of inductive and resonance effects. For example, while acenes and dihydrophenazines are donor materials, diazapentacenes are electron-transport materials due to nitrogen's greater electronegativity.^{5,6} In nitrogen-doped graphene nanoribbons, carbazole and phenanthridine subunits act as p- and n-type dopants, respectively, and the thermal rearrangement of one to another creates an intrinsic heterojunction.⁷ Nitrogen functionalization of π -conjugated systems has enhanced a variety of additional applications including energy storage, catalysis, and sensing.^{8–10}

In oligosilanes and polysilanes, small molecules and polymers containing Si–Si bonds, the overlap of σ -orbitals gives rise to σ -conjugation.^{11,12} Oligosilanes have lower energy optical transitions than alkanes and show a progressive narrowing of the HOMO–LUMO gap with increasing numbers of Si atoms.¹³ Chemical structures that combine σ - and π -conjugation, such as phenyl-terminated oligosilanes, show further bathochromic shifts in absorption.¹³ The σ, π -conjugation phenomenon has been explored in the development of conductive polymers based on polymethylphenylsilane.^{14,15} We recently reported a novel class of σ, π -hybrid compounds that are promising candidates for charge transport materials and switchable optoelectronic devices.^{16–18} Ultrafast spectroscopic characterization demonstrated that these materials undergo intramolecular charge transfer from the σ -conjugated Si donor chain to the π -conjugated acceptor group.^{19,20}

The incorporation of p-orbital-bearing heteroatoms into σ -conjugated silanes is an intriguing avenue for exploration

because of the analogy to p- and n-type doping of the bulk semiconductor. Boron-functionalized polymers have been reported by Matsumi and others,^{21,22} while we recently reported the synthesis and optical characterization of SiB cycles.²³ In these cases, density functional theory (DFT) calculations have supported both the mixing of σ - and p-orbitals (p, σ -conjugation) and charge transfer.

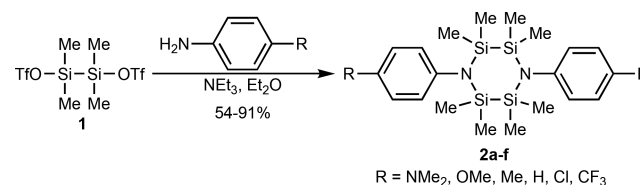
The relationship between SiN heterocycle structure and electronic properties is poorly understood, as studies of cyclic SiN compounds (silazanes)^{24–26} have focused on their use as precursors to polysilazanes^{27–29} by ring-opening polymerization and silicon nitride ceramics by pyrolysis.^{30,31} In particular, the influence of nitrogen substituents is underexplored.^{32,33}

Here, we investigate how nitrogen couples σ - and π -conjugated fragments in N-aryl substituted cyclosilazanes. Synthetic and X-ray crystallographic studies are reported. Optical properties are systematically investigated through both experimental and computational studies.

RESULTS AND DISCUSSION

Synthesis. Cyclosilazane synthesis was achieved through the reaction of bifunctional silyl triflate **1** with *para*-substituted anilines in the presence of triethylamine (NET₃) by adaptation of a procedure reported by Schmidbauer (Scheme 1).^{34,35}

Scheme 1. Synthesis of Cyclosilazanes



Received: April 21, 2019

Compound **1** is commercially available and can also be readily prepared by acid-mediated dearylation of known Ph-(SiMe₂)₂Ph.^{36,37} Competitive condensation polymerization of the primary amine with **1** was not observed. The reaction of 1,2-dichloro-1,1,2,2-tetramethyldisilane under otherwise similar reaction conditions gave lower yields and monosilylation of the aniline. Cyclosilazanes **2b–2f** were highly crystalline white solids, while **2a** was a yellow solid.

X-ray Crystallography. Given the strong dependence of oligosilane absorption spectra on conformation,³⁸ we sought structural insight into the cyclosilazanes via X-ray crystallography. Crystals of **2a–2f** suitable for X-ray structure determination were grown from Et₂O/MeCN at room temperature or –30 °C (see the [Experimental section](#)). Crystal structures are shown in [Figure 1](#). [Table 1](#) summarizes selected structural parameters.

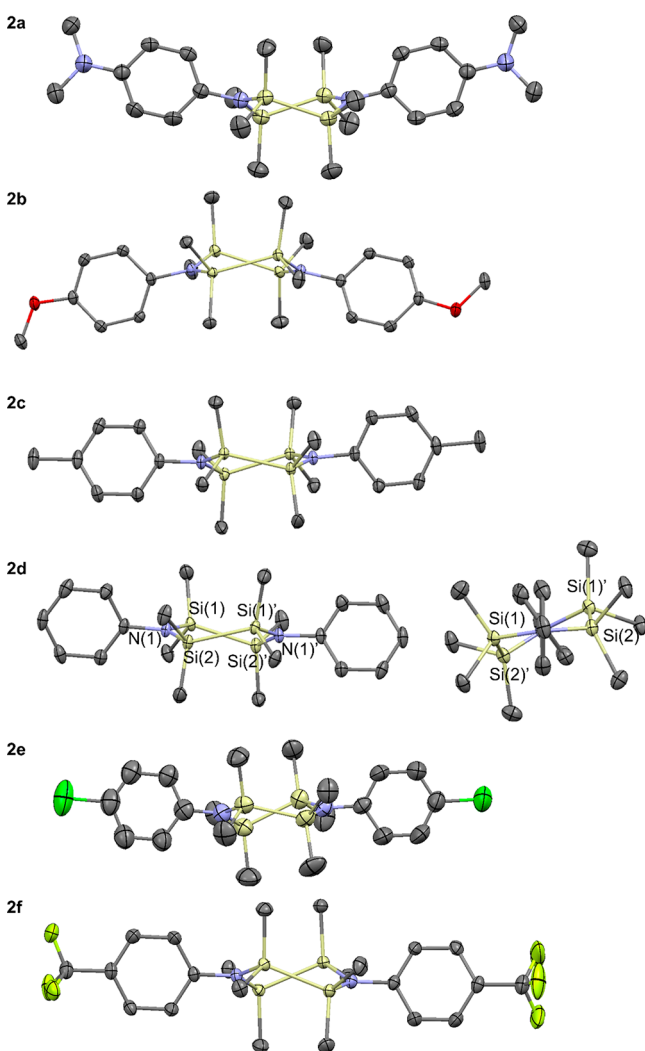


Figure 1. Crystal structures of compounds showing a molecule of compounds **2a–2f**. Hydrogens and disorder (for compounds **2e** and **2f** only) are omitted for clarity. View through the N(1)–N(1)' axis included for **2d**. Yellow = silicon, blue = nitrogen, gray = carbon, red = oxygen, lime green = chlorine, yellow-green = fluorine. The asymmetric unit for **2e** has two crystallographically independent molecules; the more disordered molecule was omitted for clarity (see the [Supporting Information](#) for details).

Table 1. Selected Geometrical Parameters for the Experimental Crystal Structures of **2a–2f**

compound	\angle Si–N–C–C ^a (deg)	Si–N bond lengths (Å)
2a	79.73(19)	1.7405(14), 1.7420(14)
2b	–75.66(16)	1.7363(12), 1.7412(12), 1.7421(12), 1.7427(12)
2c	84.57(13)	1.7384(11), 1.7384(11)
2d	83.00(19)	1.7388(14), 1.7434(13)
2e	74.2(4)	molecule A: 1.741(3), 1.742(3), 1.746(3), 1.748(3) molecule B: 1.741(7), 1.744(14), 1.748(7), 1.761(15)
2f	70.3(2)	1.7483(15), 1.7504(16), 1.7521(16), 1.7538(17)

^aTorsion angle; the smallest torsion angle was selected.

Crystal structures of **2a–2f** exhibit characteristic features of a twist-boat conformation.³⁹ Excluding the aryl groups, the cyclosilazane ring has an approximate *D*₂ symmetry ([Figure S1](#)). All silazane nitrogens on **2a–2f** adopt a trigonal planar geometry with the sum of all three nitrogen bond angles >359.6°. Looking down the N(1)–N(1)' axis of **2d** ([Figure 1](#)) shows that N(1) and N(1)' are coplanar with Si(1) and Si(2) while Si(1)' and Si(2)' are displaced away from the plane in opposite directions. Compounds **2a–2f** exhibit typical bond lengths for both Si–N (1.736–1.752 Å) and Si–Si (2.347–2.357 Å) single bonds.⁴⁰ Schmidbauer et al. reported a cyclosilazane structure where nitrogen is substituted with a *t*Bu group and silicon is bound to hydrogen rather than methyl groups.³⁴ Their cyclosilazane also adopts a twist-boat conformation where the two nitrogen atoms adopt a nearly planar configuration and the Si–Si bond distances are similar.

Aryl groups on **2a–2f** are nearly perpendicular to the Si–N–Si plane (torsion angles 70.3–84.6°, [Table 1](#)). An energy scan calculation was performed on **2d** ([Figure S2](#)). An energy minimum was found at a Si–N–C–C torsion angle of 96.0°, while an energy maximum was found at a torsion angle of 16.0°. The difference in the energy minimum and maximum was 10.04 kcal/mol. These results suggest that the energetic penalty of steric interactions between the Si–Me groups and ortho C–H bonds on the aryl groups are more significant than electron delocalization between the N lone pair and π system of the aryl ring.

UV–vis Spectroscopy. Cyclosilazane optical properties were investigated to elucidate structure–property relationships. UV–vis absorption spectra of **2a–2f** were recorded in *n*-pentane at room temperature ([Figure 2](#)). The absorption spectrum of **2d** was blue-shifted by 43 nm relative to aniline ([Figure S3](#)). The twisting of the nitrogen atom out of planarity upon silylation likely accounts for the blue shift. In acidic media, aniline's absorption spectrum undergoes an ~30 nm hypsochromic shift due to nitrogen protonation and loss of conjugation.⁴¹

All six cyclosilazanes exhibited three absorption bands (λ , [Table 2](#)). Analysis of structure–property relationships suggested that the highest energy feature involves the sigma framework, while lower energy transitions include the aromatic moiety. The position of the highest energy transition (194–201 nm) was largely insensitive to the aryl substituent. The position of the second transition for compounds bearing electron-donating substituents **2a, b** (232–261 nm) was red-shifted relative to **2c–2f** (218–226 nm). The lowest energy

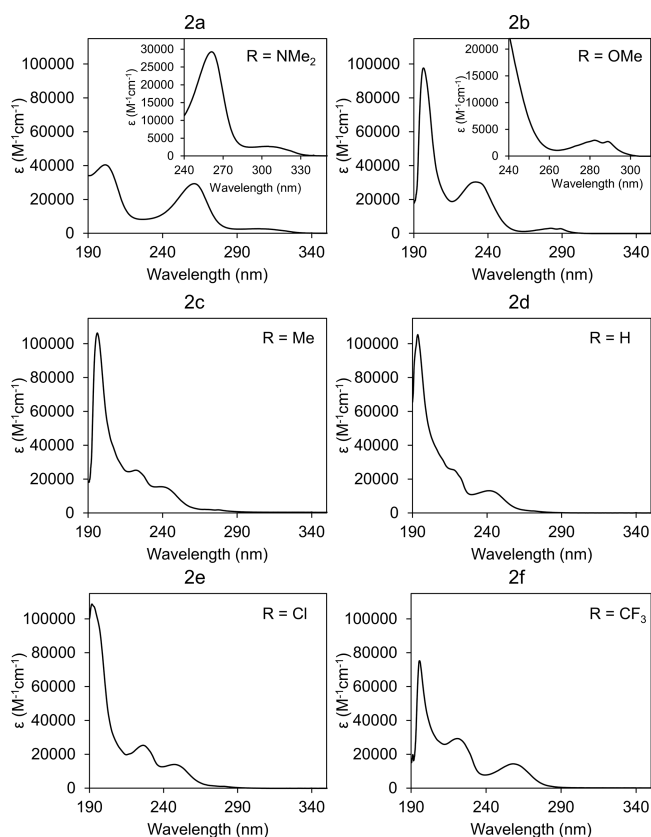


Figure 2. UV–visible absorbance spectra of **2a–2f**. Spectra recorded in *n*-pentane at room temperature ($[analyte] = 1.0 \times 10^{-5} \text{ M}$).

Table 2. Onset of Absorbance and Optical Band Gap for **2a–2f**

compound	λ (nm)	λ_{onset}^a (nm)	E_g^b (eV)
2a	203, 261, 305	333	3.72
2b	197, 232, 289	299	4.14
2c	196, 222, 239	257	4.82
2d	194, 218, 242	260	4.76
2e	196, 226, 247	265	4.67
2f	196, 221, 258	279	4.44

^a λ_{onset} = wavelength of light corresponding to the onset of absorbance.
^b E_g = optical band gap.

feature is also influenced by the aromatic substituent. Compounds with NMe₂, OMe, and CF₃ substituents (**2a**, **2b**, and **2f**) are bathochromically shifted (258–305 nm) relative to compounds with weak donors and acceptors (**2c–2e**, 239–247 nm).

More polar solvents (THF, CH₂Cl₂, MeCN) were also investigated (Figures S4–S6). Modest solvatochromism was apparent in the lowest energy transition, with a ca. 5 nm bathochromic shift from the least to the most polar solvent.

Cyclic Voltammetry and Density Functional Theory (DFT). Cyclic voltammetry (CV), coupled to computational studies, was pursued to further probe cyclosilazane substituent effects. Energies were referenced to ferrocene (Fc). Irreversible oxidation was observed for all compounds. The onset of oxidation increased as the substituent became more electron withdrawing (Table 3). The HOMO energy was calculated from eq 1, where $E_{\text{onset}}^{\text{ox}}$ is the onset of oxidation of the analyte, 4.8 eV is the HOMO energy of ferrocene below

Table 3. Electrochemical Data for **2a–2f**

compound	$E_{\text{onset}}^{\text{ox}a}$ (V)	HOMO ^b (eV)	LUMO ^c (eV)
2a	0.093 ^d	−4.879 ^e	−1.155
2b	0.431	−5.304	−1.157
2c	0.562	−5.427	−0.602
2d	0.567	−5.435	−0.666
2e	0.659	−5.522	−0.843
2f	0.822	−5.692	−1.248

^aOnset of oxidation (vs Fc/Fc+). ^bHOMO energy calculated from eq 1. ^cLUMO energy calculated from the HOMO energy and optical band gap. ^d $E_{\text{onset}}^{\text{ox}}$ relative to Ag/Ag+. ^e $E_{\text{onset}}^{\text{ox}}$ relative to Fc/Fc+ could not be determined due to overlap (see Figures S34 and S35). ^cCalculated from eq 1 with $E_{\text{onset}}^{\text{ox}}$ of **2a** from Figure S34 and $E_{\text{onset}}^{\text{ox}}$ of Fc from Figure S35.

vacuum, and X is the onset of oxidation of ferrocene under the CV conditions (see the Experimental Section).⁴²

$$\text{HOMO} = [-E_{\text{onset}}^{\text{ox}} - (4.8 - X)] \text{ eV} \quad (1)$$

A linear relationship ($R^2 = 0.95$, Figure 3a, solid line) was observed between the HOMO energy and the Hammett

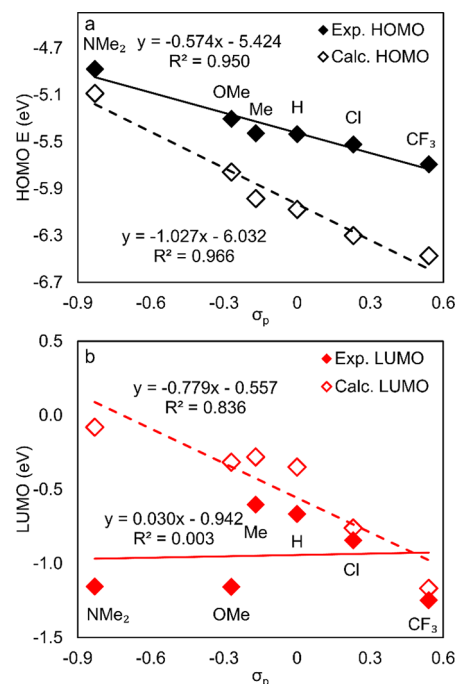


Figure 3. Experimental (solid) and theoretical (dashed) energy levels (eV) for the HOMO (a) and LUMO (b) with respect to the Hammett σ_p value for cyclosilazanes **2a–2f**. Theoretical energy levels were calculated at the B3LYP/6-311G(d) level.

parameter σ_p .^{43–45} While the voltammograms of **2a–2f** exhibit oxidation peaks, no reduction peaks were observed for **2b–2f**, complicating direct electrochemical determination of the LUMO energy (see the Supporting Information). The LUMO energy was estimated from the optical band gap and the electrochemical HOMO energy (Table 3). In this case, no linear relationship ($R^2 = 0.003$, Figure 3b, solid line) is observed between the LUMO energy and σ_p . The LUMO energy is lowered when the R group is either a strong electron donor (**2a,b**) or a strong electron acceptor (**2f**).

DFT calculations provided insight into the origin of substituent effects in cyclosilazanes. Geometry optimization

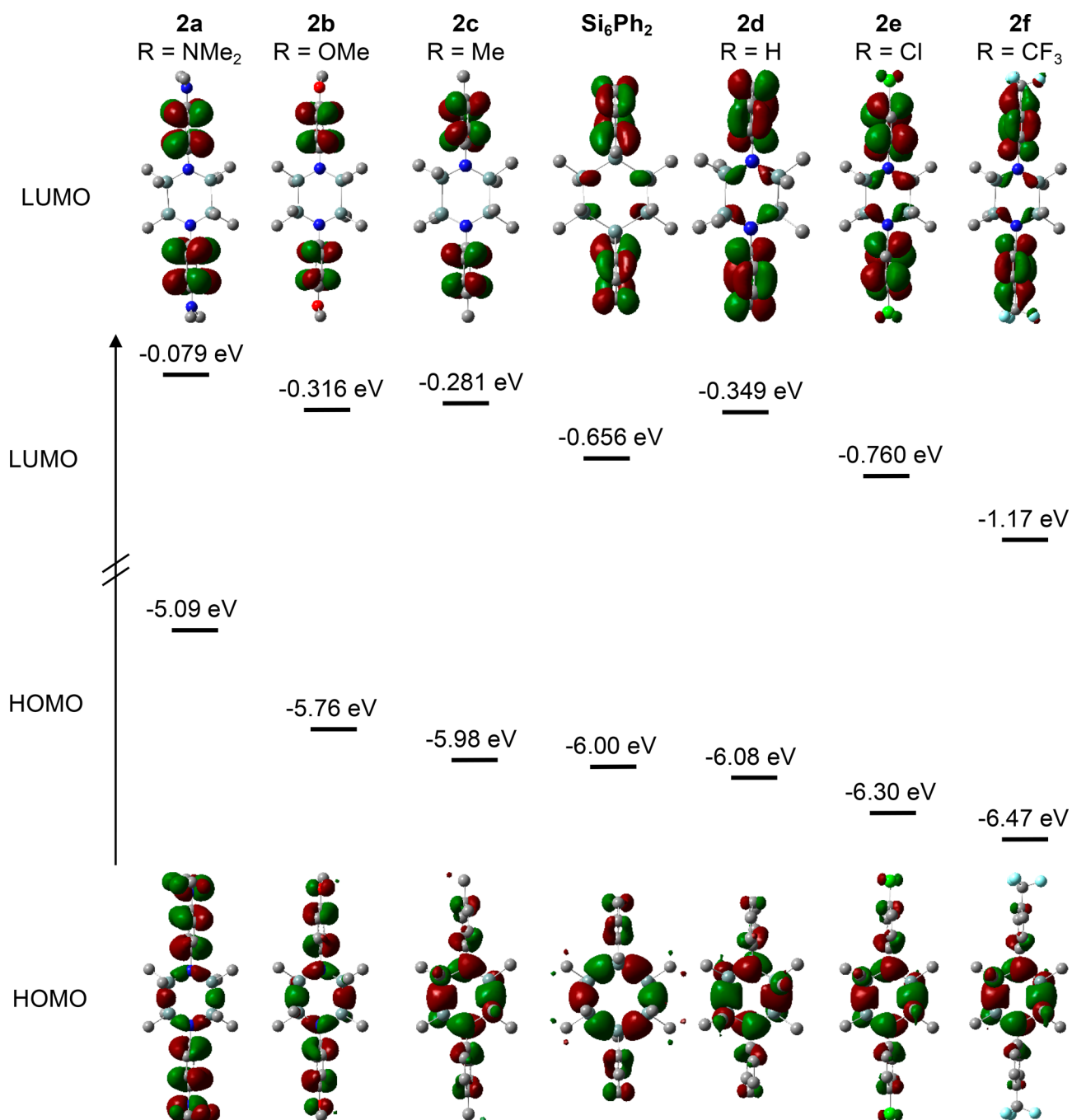


Figure 4. Calculated HOMO/LUMO orbital densities of **2a–2f** and **Si₆Ph₂**. Initial geometries were obtained from the corresponding crystal structure for **2a–2f**. Hydrogens omitted for clarity. Gray = carbon, teal = silicon, blue = nitrogen, red = oxygen, green = chlorine, light blue = fluorine. B3LYP/6-311G(d).

was performed using the crystal structures as a starting point (B3LYP/6-311G(d)). B3LYP/6-311G(d) was selected to allow for comparison to the literature, as Michl et al. reported analysis of linear alkylsilanes with this basis set and functional.⁴⁶ Significant changes were not observed at higher levels of theory.

Good agreement was observed between calculated and experimental HOMO energies (Figure 3a, compare the solid and dashed lines). Both showed a linear relationship between the Hammett parameter σ_p and the HOMO energy. The agreement between theory and experiment was less strong for the LUMO energies (Figure 3b), but the overall good

agreement between calculated and experimental HOMO–LUMO gap and λ_{onset} (see Figure S7) suggested that the computational results were of sufficient accuracy.

TD-DFT calculations of **2d** with the CAM-B3LYP functional support the involvement of the HOMO–LUMO transition in the low energy features (see Figure S8 and Table S1). We found that the CAM-B3LYP functional outperformed PBE0 and B3LYP at predicting the overall absorption spectrum of **2d**, although the predicted spectrum was hypsochromically shifted by ca. 15 nm relative to experiment.

Calculated HOMO and LUMO isodensity plots are shown in Figure 4. In all cases, HOMO orbital density is seen on both the σ and π fragments of the cyclosilazane. This suggests that nitrogen can effectively couple these fragments in the HOMO. The degree of σ - π coupling is substituent dependent. As the aromatic substituent becomes less electron-donating, the HOMO orbital density on the anilinic component lessens, and in **2f** (R = CF₃), the HOMO density is mostly concentrated on the silazane ring. At the other extreme, the compound with the most electron-donating substituent (**2a**, R = NMe₂) has a different HOMO isodensity plot from the other compounds in the series. For compounds **2b**-**2f**, a nitrogen p-orbital is apparent and bridges the conjugation associated with the Si-Si σ -conjugation and the aromatic π -system, while the **2a** HOMO does not include a nitrogen p-orbital and exhibits σ - π conjugated structure similar to an all Si analogue (Figure S9).

Only in some cases is LUMO orbital density seen on both the SiN and aromatic ring: all compounds have LUMO density on the aromatic ring, while only comparatively electron-poor substituents **2d**-**2f** show orbital density on the SiN system. This likely accounts for the weaker linear free energy relationship between σ_p and experimental LUMO energies.

Finally, we sought to understand how SiN rings **2a**-**2f** compare to all silicon rings, in analogy to the n-type doping of bulk silicon by elements from group V. Quantum chemical calculations shed light on how nitrogen incorporation perturbs HOMO and LUMO energies in cyclosilanes. *trans*-1,4-Diphenyldecamethylcyclohexasilane (Si₆Ph₂) was selected as a control compound for these computational studies. Si₆Ph₂ and its cyclosilazane analogue **2d** have HOMOs of similar energy, although the LUMO of **2d** is ca. 0.3 eV higher in energy. Electron-withdrawing substituents shift both HOMO and LUMO energies down, while electron-donating substituents shift HOMO and LUMO energies up relative to Si₆Ph₂ (Figure 4). Thus, depending on the aromatic substituent, the effect of nitrogen incorporation can be n- or p-type.

CONCLUSION

In conclusion, we have demonstrated a high yielding synthesis of N-aryl cyclosilazanes. We varied the *para*-substituent of the anilinic subunit in the cyclosilazanes and spectroscopically and electronically investigated substituent effects. Our experimental and computational results showed that the aniline substituent systematically perturbs HOMO energies. A Hammett analysis of the silazane energies revealed a correlation of σ_p with the HOMO energy. Calculations of HOMO/LUMO densities revealed the nitrogen nonbonding p-orbital can bridge σ - and π -conjugated systems and that SiN rings can be tuned to either more or less electron rich than all silicon rings.

EXPERIMENTAL SECTION

General Procedures. All experiments were performed using either standard Schlenk line techniques under a dry argon atmosphere or a UNILab Plus Glove Box by MBRAUN under a dry nitrogen atmosphere. All glassware was oven-dried overnight in a 175 °C oven. All reaction solvents were dried and degassed on a J. C. Meyer Solvent Dispensing System. Granular lithium, triethylamine, isopropylmagnesium chloride (2 M in THF), dichlorodimethylsilane, aniline, *p*-toluidine, 4-chloroaniline, *p*-anisidine, 4-(trifluoromethyl)aniline, tetrabutylammonium tetrafluoroborate (TBABF₄), ferrocene, and anhydrous acetonitrile were purchased from Sigma-Aldrich. Trifluoromethanesulfonic acid (triflic acid, TfOH) was purchased from Acros

Organics. Chloro(dimethyl)phenylsilane was purchased from Gelest. *p*-Toluidine, *p*-chloroaniline, and *p*-anisidine were sublimed under a vacuum prior to use. NEt₃ was freshly distilled from KOH under Ar prior to use. TBABF₄ was recrystallized from an 80/20 (v/v) water/ethanol mixture. Ferrocene was sublimed at 100 °C. Compound **1** was synthesized from known Ph(SiMe₂)₂Ph which was prepared by adaptation of a literature procedure.⁴⁷ All other chemicals were obtained from commercial suppliers and used without further purification. ¹H NMR, ¹³C {¹H} NMR, ²⁹Si {¹H} NMR, and ¹⁹F {¹H} NMR spectra were recorded on a Bruker Avance 300 or 400 MHz Spectrometer, and chemical shifts are reported in parts per million (ppm). NMR spectra were recorded in CDCl₃ with tetramethylsilane (TMS) or the residual solvent as the internal standard (¹H NMR: CHCl₃ δ = 7.26). Multiplicities are as indicated: s (singlet), q (quartet), p (pentet), and m (multiplet). Coupling constants, *J*, are reported in Hertz, and integration is provided. High resolution mass spectrometry (HRMS) was performed at the Columbia University mass spectrometry facility using a Waters XEVO 62XS QToF mass spectrometer equipped with a UPC2 SFC inlet, electrospray ionization (ESI) probe, atmospheric pressure chemical ionization (APCI) probe, and atmospheric solids analysis probe (ASAP). All column chromatography was performed on a Teledyne ISCO Combiflash Rf+ using Redisep Rf silica columns. Elemental analysis was performed by Robertson Microлит Laboratories. For **2b** and **2d**, carbon content was lower than expected by more than 0.4%. Although these results are outside the range viewed as establishing analytical purity, they are provided to illustrate the best values obtained to date. Additionally, low carbon content in organosilane elemental analysis has previously been attributed to incomplete combustion related to SiC formation.^{48,49} UV-vis spectroscopy was performed on a Shimadzu UV-1800 UV-vis spectrophotometer. The UV-vis spectra were measured at room temperature in pentane in a quartz cuvette (10 mm). Cyclic voltammetry (CV) measurements were performed inside a glovebox under a dry nitrogen atmosphere. CV measurements were obtained with a CH Instruments, Inc., 600 E Electrochemical Analyzer with a 2 mm diameter platinum working electrode, a platinum wire counter electrode, and a quasi-internal silver wire reference electrode submerged in 0.01 M AgNO₃/0.1 M TBABF₄ in anhydrous acetonitrile. Voltammograms were obtained with an analyte concentration of 3.5 mM and 0.1 M TBABF₄ in anhydrous acetonitrile with a scan rate of 100 mV s⁻¹ using ferrocene as an internal reference.

Synthesis of 1,2-Diphenyl-1,1,2,2-tetramethyldisilane (Ph(SiMe₂)₂Ph). Chloro(dimethyl)phenylsilane (4.0 mL, 23.7 mmol) was added dropwise to a Schlenk flask containing lithium granules (0.66 g, 95.1 mmol) suspended in THF (24 mL) at 0 °C. After complete addition, the reaction was warmed to room temperature and stirred overnight. The next day, the solution was filtered under Ar to another Schlenk flask. *i*PrMgCl (2 M in THF, 11.9 mL, 23.7 mmol) was added to the filtrate at 0 °C dropwise and stirred for 20 min. Chloro(dimethyl)phenyl-silane (4.0 mL, 23.7 mmol) was added and stirred at room temperature for 3 h. The reaction mixture was quenched at 0 °C by dropwise addition of water followed by saturated ammonium chloride solution. The aqueous and organic layers were separated, and the aqueous layer was extracted three times with Et₂O. The combined Et₂O layers were washed with brine solution followed by Na₂SO₄ before being concentrated by rotary evaporation to yield a yellow liquid. Purification was achieved by column chromatography on silica gel with hexanes to yield a white solid (4.61 g, 72%). NMR spectra agree with a previous report.⁵⁰

Synthesis of 1,2-Bis(trifluoromethanesulfonate)-tetramethyl-disilane (1). Triflic acid (8.03 mL, 90.7 mmol) was added dropwise via addition funnel to 1,2-diphenyl-1,1,2,2-tetramethyldisilane (12.26 g, 45.4 mmol) dissolved in dichloromethane (75 mL) at 0 °C. The reaction was stirred at 0 °C for 30 min followed by room temperature for 1 h. Volatile materials were removed under a vacuum to yield a yellow liquid. The resulting compound was distilled from the crude liquid under a vacuum (45 °C, 0.7 Torr) to yield a colorless liquid (18.72 g, 99%). ¹H NMR (400 MHz, CDCl₃) δ 0.73

(s, 12H). ^{13}C $\{^1\text{H}\}$ (101 MHz, CDCl_3) δ 118.3 (q, $J = 317.7$ Hz), -0.6 (s). ^{29}Si $\{^1\text{H}\}$ NMR (79 MHz, CDCl_3) δ 33.6. ^{19}F $\{^1\text{H}\}$ (282 MHz, CDCl_3) δ -75.90 .

General Procedure for the Synthesis of 2a–2f. Disilane **1** (1.00 g, 2.41 mmol) was added dropwise via syringe to the corresponding substituted aniline (2.41 mmol) and NEt_3 (0.68 mL, 4.82 mmol) dissolved in Et_2O (24 mL) and stirred at room temperature for 2 h. A biphasic mixture formed after stirring for 30 min. After 2 h, the bottom ionic liquid layer was frozen at -78 °C. The top Et_2O layer was cannulated to an oven-dried Schlenk flask, and volatile materials were removed under a vacuum to yield the crude cyclosilazane.

Synthesis of 2a. Synthesized according to the above general procedure (0.330 g of *N,N*-dimethyl-*p*-phenylenediamine). Pure **2a** was obtained by slow evaporation recrystallization in $\text{Et}_2\text{O}/\text{MeCN}$ at room temperature (0.512 g, 85%). ^1H NMR (400 MHz, CDCl_3) δ 6.78 (d, $J = 8.9$ Hz, 4H), 6.65 (d, $J = 8.9$ Hz, 4H), 2.91 (s, 12H), 0.09 (s, 24H). ^{13}C $\{^1\text{H}\}$ (101 MHz, CDCl_3) δ 147.4, 135.4, 130.5, 113.3, 41.3, 0.7. ^{29}Si $\{^1\text{H}\}$ NMR (79 MHz, CDCl_3) δ -6.8 . HRMS (ASAP+) Calcd [M + H] for $\text{C}_{24}\text{H}_{44}\text{N}_4\text{Si}_4$ 501.2721, found 501.2727. Anal. Calcd for $\text{C}_{24}\text{H}_{44}\text{N}_4\text{Si}_4$: C, 57.54; H, 8.85; N, 11.18. Found: C, 57.33; H, 8.99; N, 11.06.

Synthesis of 2b. Synthesized according to the above general procedure (0.308 g of *p*-anisidine). Pure **2b** was obtained by recrystallization in MeCN at -30 °C (0.361 g, 63%). ^1H NMR (400 MHz, CDCl_3) δ 6.85–6.76 (m, 8H), 3.79 (s, 6H), 0.10 (s, 24H). ^{13}C $\{^1\text{H}\}$ (101 MHz, CDCl_3) δ 156.2, 138.6, 130.7, 114.0, 55.5, 0.6. ^{29}Si $\{^1\text{H}\}$ NMR (79 MHz, CDCl_3) δ -6.5 . HRMS (ASAP+) Calcd [M + H] for $\text{C}_{22}\text{H}_{38}\text{O}_2\text{N}_2\text{Si}_4$ 475.2089, found 475.2095. Anal. Calcd for $\text{C}_{22}\text{H}_{38}\text{O}_2\text{N}_2\text{Si}_4$: C, 55.64; H, 8.07; N, 5.90. Found: C, 54.22; H, 7.79; N, 5.69.

Synthesis of 2c. Synthesized according to the above general procedure (0.259 g of *p*-toluidine). Pure **2c** was obtained by slow evaporation recrystallization in $\text{Et}_2\text{O}/\text{MeCN}$ at room temperature (0.405, 76%). ^1H NMR (400 MHz, CDCl_3) δ 7.07–7.01 (m, 4H), 6.82–6.77 (m, 4H), 2.31 (s, 6H), 0.11 (s, 24H). ^{13}C $\{^1\text{H}\}$ (101 MHz, CDCl_3) δ 143.1, 133.0, 129.7, 129.4, 21.0, 0.7. ^{29}Si $\{^1\text{H}\}$ NMR (79 MHz, CDCl_3) δ -6.6 . HRMS (ASAP+) Calcd [M + H] for $\text{C}_{22}\text{H}_{38}\text{N}_2\text{Si}_4$ 443.2190, found 443.2190. Anal. Calcd for $\text{C}_{22}\text{H}_{38}\text{N}_2\text{Si}_4$: C, 59.66; H, 8.65; N, 6.33. Found: C, 59.39; H, 8.80; N, 6.19.

Synthesis of 2d. Synthesized according to the above general procedure (0.22 mL of aniline). Pure **2d** was obtained by recrystallization in MeCN at -30 °C (0.455 g, 91%). ^1H NMR (400 MHz, CDCl_3) δ 7.27–7.22 (m, 4H), 7.10–7.05 (m, 2H), 6.94–6.89 (m, 4H), 0.13 (s, 24H). ^{13}C $\{^1\text{H}\}$ (101 MHz, CDCl_3) δ 146.1, 129.8, 128.8, 123.7, 0.7. ^{29}Si $\{^1\text{H}\}$ NMR (79 MHz, CDCl_3) δ -6.2 . HRMS (ASAP+) Calcd [M + H] for $\text{C}_{20}\text{H}_{34}\text{N}_2\text{Si}_4$ 415.1877, found 415.1873. Anal. Calcd for $\text{C}_{20}\text{H}_{34}\text{N}_2\text{Si}_4$: C, 57.91; H, 8.26; N, 6.75. Found: C, 57.13; H, 8.02; N, 6.54.

Synthesis of 2e. Synthesized according to the above general procedure (0.308 g of *p*-chloroaniline). Pure **2e** was obtained by slow evaporation recrystallization in $\text{Et}_2\text{O}/\text{MeCN}$ at room temperature (0.379 g, 65%). ^1H NMR (400 MHz, CDCl_3) δ 7.24–7.18 (m, 4H), 6.87–6.80 (m, 4H), 0.12 (s, 24H). ^{13}C $\{^1\text{H}\}$ (101 MHz, CDCl_3) δ 144.7, 130.9, 129.3, 129.0, 0.6. ^{29}Si $\{^1\text{H}\}$ NMR (79 MHz, CDCl_3) δ -5.7 . HRMS (ASAP+) Calcd [M + H] for $\text{C}_{20}\text{H}_{32}\text{Cl}_2\text{N}_2\text{Si}_4$ 483.1098, found 483.1106. Anal. Calcd for $\text{C}_{20}\text{H}_{32}\text{Cl}_2\text{N}_2\text{Si}_4$: C, 49.66; H, 6.67; N, 5.79. Found: C, 49.87; H, 6.57; N, 5.79.

Synthesis of 2f. Synthesized according to the above general procedure (0.31 mL of 4-(trifluoromethyl)aniline). Pure **2f** was obtained by recrystallization in MeCN at -30 °C (0.360 g, 54%). ^1H NMR (400 MHz, CDCl_3) δ 7.51 (d, $J = 8.2$ Hz, 4H), 7.01 (d, $J = 8.2$ Hz, 4H), 0.17 (s, 24H). ^{13}C NMR $\{^1\text{H}\}$ (101 MHz, chloroform-*d*) δ 150.2 (q, $J = 1.3$ Hz), 129.4 (s), 126.1 (q, $J = 3.7$ Hz), 126.0 (q, $J = 271.7$ Hz), 125.9 (q, $J = 32.5$ Hz), 0.7 (s). ^{29}Si $\{^1\text{H}\}$ NMR (79 MHz, CDCl_3) δ -5.0 , ^{19}F $\{^1\text{H}\}$ NMR (282 MHz, CDCl_3) δ -61.33 . HRMS (ASAP+) Calcd [M + H] for $\text{C}_{22}\text{H}_32\text{F}_6\text{N}_2\text{Si}_4$ 551.1625, found 551.1620. Anal. Calcd for $\text{C}_{22}\text{H}_32\text{F}_6\text{N}_2\text{Si}_4$: C, 47.97; H, 5.86; N, 5.09. Found: C, 48.14; H, 5.71; N, 5.00.

Computational Details. All calculations were carried out using the Gaussian 09 package.⁵¹ Geometries were optimized from the crystal structure using the B3LYP functional with the 6-311G(d) basis set with forced nonsymmetry. All optimized structures possess zero imaginary frequencies. The TD-DFT calculation of **2d** was performed using the CAM-B3LYP functional with the 6-311G(d) basis set using the geometry optimized coordinates of **2d** from the B3LYP/6-311G(d) functional. The 20 lowest excitations were calculated.

■ ASSOCIATED CONTENT

Supporting Information

The Supporting Information is available free of charge on the ACS Publications website at DOI: 10.1021/acs.organomet.9b00254.

Computed Cartesian coordinates of all of the molecules reported in this study (XYZ)

NMR spectra of compounds **1** and **2a–2f**, cyclic voltammograms, crystal measurement and refinement data for compounds studied by XRD, and TD-DFT results (PDF)

Accession Codes

CCDC 1892007–1892012 contain the supplementary crystallographic data for this paper. These data can be obtained free of charge via www.ccdc.cam.ac.uk/data_request/cif, or by emailing data_request@ccdc.cam.ac.uk, or by contacting The Cambridge Crystallographic Data Centre, 12 Union Road, Cambridge CB2 1EZ, UK; fax: +44 1223 336033.

■ AUTHOR INFORMATION

Corresponding Author

*E-mail: klausen@jhu.edu.

ORCID

Maxime A. Siegler: 0000-0003-4165-7810

Rebekka S. Klausen: 0000-0003-4724-4195

Notes

The authors declare no competing financial interest.

■ ACKNOWLEDGMENTS

This work was supported by the U.S. Department of Energy (DOE), Office of Science, Basic Energy Sciences under Award No. DE-SC0013906 (molecular synthesis). DFT calculations were conducted using scientific computing services at the Maryland Research Computing Center (MARCC). We thank Prof. Lan Cheng (Johns Hopkins University) for helpful discussions.

■ REFERENCES

- (1) He, X.; Baumgartner, T. Conjugated Main-Group Polymers for Optoelectronics. *RSC Adv.* **2013**, *3*, 11334–11350.
- (2) Emanuelsson, R.; Denisova, A. V.; Baumgartner, J.; Ottosson, H. Optimization of the Cyclic Cross-Hyperconjugation in 1,4-Diethylcyclohexa-2,5-Dienes. *Organometallics* **2014**, *33*, 2997–3004.
- (3) Stolar, M.; Baumgartner, T. Functional Conjugated Pyridines via Main-Group Element Tuning. *Chem. Commun.* **2018**, *54*, 3311–3322.
- (4) Durr, R. A.; Haberer, D.; Lee, Y. L.; Blackwell, R.; Kalayjian, A. M.; Marangoni, T.; Ihm, J.; Louie, S. G.; Fischer, F. R. Orbital-Matched Edge-Doping in Graphene Nanoribbons. *J. Am. Chem. Soc.* **2018**, *140*, 807–813.
- (5) Tang, X.-D.; Liao, Y.; Geng, H.; Shuai, Z.-G. Fascinating Effect of Dehydrogenation on the Transport Properties of N-Heteropentacenes: Transformation From *p*- to *n*-Type Semiconductor. *J. Mater. Chem.* **2012**, *22*, 18181–18191.

- (6) Appleton, A. L.; Brombosz, S. M.; Barlow, S.; Sears, J. S.; Bredas, J.-L.; Marder, S. R.; Bunz, U. H. F. Effects of Electronegative Substitution on the Optical and Electronic Properties of Acenes and Diazaacenes. *Nat. Commun.* **2010**, *1*, 91.
- (7) Marangoni, T.; Haberer, D.; Rizzo, D. J.; Cloke, R. R.; Fischer, F. R. Heterostructures through Divergent Edge Reconstruction in Nitrogen-Doped Segmented Graphene Nanoribbons. *Chem. - Eur. J.* **2016**, *22*, 13037–13040.
- (8) Inagaki, M.; Toyoda, M.; Soneda, Y.; Morishita, T. Nitrogen-Doped Carbon Materials. *Carbon* **2018**, *132*, 104–140.
- (9) Wood, K. N.; O'Hayre, R.; Pylypenko, S. Recent Progress on Nitrogen/Carbon Structures Designed for Use in Energy and Sustainability Applications. *Energy Environ. Sci.* **2014**, *7*, 1212–1249.
- (10) Wang, H.; Maiyalagan, T.; Wang, X. Review on Recent Progress in Nitrogen-Doped Graphene: Synthesis, Characterization, and Its Potential Applications. *ACS Catal.* **2012**, *2*, 781–794.
- (11) Miller, R. D.; Michl, J. Polysilane High Polymers. *Chem. Rev.* **1989**, *89*, 1359–1410.
- (12) Marro, E. A.; Klausen, R. S. Conjugated Polymers Inspired by Crystalline Silicon. *Chem. Mater.* **2019**, *31*, 2202–2211.
- (13) Gilman, H.; Atwell, W. H.; Schwebke, G. L. Ultraviolet Properties of Compounds Containing the Silicon-Silicon Bond. *J. Organomet. Chem.* **1964**, *2*, 369–371.
- (14) West, R.; David, L. D.; Djurovich, P. I.; Stearley, K. L.; Srinivasan, K. S. V.; Yu, H. Phenylmethylpolysilanes: Formable Silane Copolymers with Potential Semiconducting Properties. *J. Am. Chem. Soc.* **1981**, *103*, 7352–7354.
- (15) Trujillo, R. E. Preparation of Long-Chain Poly-(Methylphenylsilane). *J. Organomet. Chem.* **1980**, *198*, C27–C28.
- (16) Surampudi, S.; Yeh, M.-L.; Siegler, M. A.; Hardigree, J. F. M.; Kasl, T. A.; Katz, H. E.; Klausen, R. S.; Seki, S.; Tibbelin, J.; Ottosson, H.; et al. Increased Carrier Mobility in End-Functionalized Oligosilanes. *Chem. Sci.* **2015**, *6*, 1905–1909.
- (17) Press, E. M.; Marro, E. A.; Surampudi, S. K.; Siegler, M. A.; Tang, J. A.; Klausen, R. S. Synthesis of a Fragment of Crystalline Silicon: Poly(Cyclosilane). *Angew. Chem., Int. Ed.* **2017**, *56*, 568–572.
- (18) Marro, E. A.; Press, E. M.; Siegler, M. A.; Klausen, R. S. Directional Building Blocks Determine Linear and Cyclic Silicon Architectures. *J. Am. Chem. Soc.* **2018**, *140*, 5976–5986.
- (19) Zhou, J.; Surampudi, S. K.; Bragg, A. E.; Klausen, R. S. Photoinduced Charge Separation in Molecular Silicon. *Chem. - Eur. J.* **2016**, *22*, 6204–6207.
- (20) Zhou, J.; Folster, C. P.; Surampudi, S. K.; Jimenez, D.; Klausen, R. S.; Bragg, A. Asymmetric Charge Separation and Recombination in Symmetrically Functionalized σ - π Hybrid Oligosilanes. *Dalt. Trans.* **2017**, *46*, 8716–8726.
- (21) Hsu, M.-T. S.; Chen, T. S.; Riccitiello, S. R. Preceramic Organoboron-Silicon Polymers. *J. Appl. Polym. Sci.* **1991**, *42*, 851–861.
- (22) Puneet, P.; Vedarajan, R.; Matsumi, N. σ -p Conjugated Copolymers via Dehydrocoupling Polymerization of Phenylsilane and Mesitylborane. *Polym. Chem.* **2016**, *7*, 4182–4187.
- (23) Purkait, T. K.; Press, E. M.; Marro, E. A.; Siegler, M. A.; Klausen, R. S. Low-Energy Electronic Transition in SiB Rings. *Organometallics* **2019**, *38*, 1688–1698.
- (24) Fink, W. Silicon-Nitrogen Heterocycles. *Angew. Chem., Int. Ed. Engl.* **1966**, *5*, 760–776.
- (25) Duguet, E.; Schappacher, M.; Soum, A. New Cyclodisilazane Monomers. *J. Organomet. Chem.* **1993**, *458*, 9–12.
- (26) Xiao, Y.; Son, D. Y. Synthetic Approaches to Cyclodisilazanes and Branched Silazanes. *Organometallics* **2004**, *23*, 4438–4443.
- (27) Duguet, E.; Schappacher, M.; Soum, A. High Molar Mass Polysilazane: A New Polymer. *Macromolecules* **1992**, *25*, 4835–4839.
- (28) Duguet, E.; Schappacher, M.; Soums, A. Cationic Ring-Opening Polymerization of Hexamethylcyclodisilazane: General Aspects and Tentative Mechanisms. *Polym. Int.* **1994**, *33*, 129–139.
- (29) Seyferth, D.; Schwark, J. M.; Stewart, R. M. Stoichiometric and Catalytic Ring Opening of Hexaalkylcyclodisilazanes by Organoalkali Reagents. *Organometallics* **1989**, *8*, 1980–1986.
- (30) Han, H. N.; Lindquist, D. A.; Haggerty, J. S.; Seyferth, D. Pyrolysis Chemistry of Poly(Organosilazanes) to Silicon Ceramics. *Chem. Mater.* **1992**, *4*, 705–711.
- (31) Birot, M.; Pillot, J. P.; Dunoguès, J. Comprehensive Chemistry of Polycarbosilanes, Polysilazanes, and Polycarbosilazanes as Precursors of Ceramics. *Chem. Rev.* **1995**, *95*, 1443–1477.
- (32) Newman, T. H.; West, R.; Oakley, R. T. Synthesis and Spectral Properties of Group V Heteroatom-Permethylocyclopolysilanes, MeN-(SiMe₂)_n and MeP(SiMe₂)_n. *J. Organomet. Chem.* **1980**, *197*, 159–168.
- (33) Watanabe, H.; Sekiguchi, Y.; Ohmori, H.; Nishiyama, M.; Sugo, M.; Yoshikawa, M.; Hirai, N.; Kanuma, Y.; Adachi, T.; Makino, M.; et al. Peralkylated Four- and Five-Membered Cyclosilanes Containing a Heteroatom: Synthesis, Structure, and Properties. *Eur. J. Inorg. Chem.* **2002**, *2002*, 1772–1793.
- (34) Söldner, M.; Schier, A.; Schmidbauer, H. 1,2-Disilanediyil Bis(Triflate), F₃CSO₃-SiH₂SiH₂-O₃SCF₃, as the Key Intermediate for a Facile Preparation of Open-Chain and Cyclic 1,1- and 1,2-Diaminodisilanes. *Inorg. Chem.* **1997**, *36*, 1758–1763.
- (35) Söldner, M.; Riede, J.; Schier, A.; Schmidbauer, H. Isomeric Cyclic Disilanediyil Dimethylhydrazines. *Inorg. Chem.* **1998**, *37*, 601–603.
- (36) Uhlig, W. Silyl Triflates - Valuable Synthetic Materials in Organosilicon Chemistry. *Chem. Ber.* **1996**, *129*, 733–739.
- (37) Matyjaszewski, K.; Chen, Y. L. Synthesis and Reactions of Silanes Containing Two Triflate Groups. *J. Organomet. Chem.* **1988**, *340*, 7–12.
- (38) Bande, A.; Michl, J. Conformational Dependence of σ -Electron Delocalization in Linear Chains: Permethylylated Oligosilanes. *Chem. - Eur. J.* **2009**, *15*, 8504–8517.
- (39) Leong, M. K.; Mastryukov, V. S.; Boggs, J. E. Structure and Conformations of Six-Membered Systems A₆H₁₂ (A = C, Si): Ab Initio Study of Cyclohexane and Cy Clo Hexasilane. *J. Phys. Chem.* **1994**, *98*, 6961–6966.
- (40) Sheldrick, W. S. Structural Chemistry of Organic Silicon Compounds. In *The Chemistry of Organic Silicon Compounds*; Patai, S., Rappoport, Z., Eds.; John Wiley & Sons, Inc.: New York, 1989; pp 227–303.
- (41) Forbes, W. F.; Leckie, I. R. Light Absorption Studies Part XIII. The Electronic Absorption Spectra of Ring-Substituted Anilines. *Can. J. Chem.* **1958**, *36*, 1371–1380.
- (42) Li, H.; Xu, L.; Tang, Y.; Tao, Y.; Xu, S.; Zheng, C.; Xing, G.; Zhou, X.; Huang, W.; Chen, R. Direct Silicon-Nitrogen Bonded Host Materials with Enhanced σ - π Conjugation for Blue Phosphorescent Organic Light-Emitting Diodes. *J. Mater. Chem. C* **2016**, *4*, 10047–10052.
- (43) Hansch, C.; Leo, A.; Taft, R. W. A Survey of Hammett Substituent Constants and Resonance and Field Parameters. *Chem. Rev.* **1991**, *91*, 165–195.
- (44) Bender, T. P.; Graham, J. F.; Duff, J. M. Effect of Substitution on the Electrochemical and Xerographic Properties of Triarylaminos: Correlation to the Hammett Parameter of the Substituent and Calculated HOMO Energy Level. *Chem. Mater.* **2001**, *13*, 4105–4111.
- (45) van de Wouw, H. L.; Lee, J. Y.; Siegler, M. A.; Klausen, R. S. Innocent BN Bond Substitution in Anthracene Derivatives. *Org. Biomol. Chem.* **2016**, *14*, 3256–3263.
- (46) Kanazawa, Y.; Tsuji, H.; Ehara, M.; Fukuda, R.; Casher, D. L.; Tamao, K.; Nakatsuji, H.; Michl, J. Electronic Transitions in Conformationally Controlled Peralkylated Hexasilanes. *ChemPhysChem* **2016**, *17*, 3010–3022.
- (47) Shibano, Y.; Sasaki, M.; Tsuji, H.; Araki, Y.; Ito, O.; Tamao, K. Conformation Effect of Oligosilane Linker on Photoinduced Electron Transfer of Tetrasilane-Linked Zinc Porphyrin-[60]Fullerene Dyads. *J. Organomet. Chem.* **2007**, *692*, 356–367.
- (48) Aghazadeh Meshgi, M.; Zitz, R.; Walewska, M.; Baumgartner, J.; Marschner, C. Tuning the Si-N Interaction in Metalated Oligosilanyl silatranes. *Organometallics* **2017**, *36*, 1365–1371.

(49) Chen, J.; Tagne Kuate, A. C.; Lalancette, R. A.; Jäkle, F. Heteroatom-Bridged *ortho*-Biferrocenes: Stereoselective Synthesis, Structural Features, and Electrochemical Properties. *Organometallics* **2016**, *35*, 1964–1972.

(50) Li, Z.; Iida, K.; Tomisaka, Y.; Yoshimura, A.; Hirao, T.; Nomoto, A.; Ogawa, A. New Entry to the Construction of Si-Si Linkages: Sm/SmI₂-Induced Efficient Reductive Coupling of Organochlorosilanes. *Organometallics* **2007**, *26*, 1212–1216.

(51) Frisch, M. J.; Trucks, G. W.; Schlegel, H. B.; Scuseria, G. E.; Robb, M. A.; Cheeseman, J. R.; Scalmani, G.; Barone, V.; Mennucci, B.; Petersson, G. A.; Nakatsuji, H.; Caricato, M.; Li, X.; Hratchian, H. P.; Izmaylov, A. F.; Bloino, J.; Zheng, G.; Sonnenberg, J. L.; Hada, M.; Ehara, M.; Toyota, K.; Fukuda, R.; Hasegawa, J.; Ishida, M.; Nakajima, T.; Honda, Y.; Kitao, O.; Nakai, H.; Vreven, T.; Montgomery, J. A., Jr.; Peralta, J. E.; Ogliaro, F.; Bearpark, M.; Heyd, J. J.; Brothers, E.; Kudin, K. N.; Staroverov, V. N.; Kobayashi, R.; Normand, J.; Raghavachari, K.; Rendell, A.; Burant, J. C.; Iyengar, S. S.; Tomasi, J.; Cossi, M.; Rega, N.; Millam, J. M.; Klene, M.; Knox, J. E.; Cross, J. B.; Bakken, V.; Adamo, C.; Jaramillo, J.; Gomperts, R.; Stratmann, R. E.; Yazyev, O.; Austin, A. J.; Cammi, R.; Pomelli, C.; Ochterski, J. W.; Martin, R. L.; Morokuma, K.; Zakrzewski, V. G.; Voth, G. A.; et al. *Gaussian 09*, revision D.01; Gaussian, Inc.: Wallingford, CT, 2009.